The Influence of Atmospheric Cloud Radiative Effects on the Large-Scale Stratospheric Circulation

Ying Li* and David W. J. Thompson

Department of Atmospheric Science, Colorado State University, Fort Collins, Colorado, USA

Yi Huang

Department of Atmospheric and Oceanic Sciences, McGill University, Montreal, Quebec, Canada

Corresponding author address: Ying Li, Department of Atmospheric Science, Colorado State University, 3915 W. Laporte Ave. Fort Collins, CO 80521

E-mail: yingli@atmos.colostate.edu

ABSTRACT

Previous studies have explored the influence of atmospheric cloud radiative effects (ACRE) on the tropospheric circulation. Here the authors explore the influence of ACRE on the stratospheric circulation. The response of the stratospheric circulation to ACRE is assessed by comparing simulations run with and without ACRE under the auspices of the Clouds On-Off Klimate Intercomparsion Experiment (COOKIE). The stratospheric circulation response to ACRE is reproducible in a range of different GCMs, and can be interpreted in the context of two components: a dynamically-driven component and a radiatively-driven component.

The dynamic component is linked to changes in the vertical flux of wave activity into the lower stratosphere and meridional wave propagation within the stratosphere. The changes in the vertical wave flux are consistent with the attendant changes in tropospheric baroclinicity and thus the amplitude of midlatitude baroclinic eddies. They account for a strengthening of the Brewer-Dobson circulation, warming in the upper polar stratosphere juxtaposed against cooling in the tropical lower stratosphere, weakening of the polar vortex, and a reduction in static stability near the tropical tropopause transition layer. The changes in meridional wave propagation account for much of the meridional structure of the stratospheric response.

The radiative component is linked to changes in the flux of longwave radiation into the lower stratosphere. The changes in radiative fluxes lead to cooling of the extratropical lower stratosphere, changes in the static stability and cloud fraction near the extratropical tropopause, and a shortening of the timescales of extratropical stratospheric variability.

The results highlight a previously overlooked pathway through which tropospheric climate influences the stratosphere.

1. Introduction

Atmospheric cloud radiative effects (ACRE) are defined as the difference between cloud radiative effects at the top of the atmosphere and the surface. They have an important influence on the vertical distribution of atmospheric diabatic heating. Hence they can have a profound impact on the atmospheric circulation in both the tropical and extratropical atmosphere.

Numerous studies have explored the influence of ACRE on the tropospheric circulation. Early numerical experiments focused on the relationships between ACRE and the mean tropical circulation (Slingo and Slingo 1988, 1991; Randall et al. 1989; Gordon 1992; Sherwood et al. 1994; Tian and Ramanathan 2002, 2003). More recent experiments have highlighted the influence of ACRE on tropical intraseasonal variability (Crueger and Stevens 2015), the El Nino/Southern Oscillation (Rädel et al. 2016) and the intertropical convergence zone (Harrop and Hartmann 2016). Recent experiments have also explored the influence of ACRE associated with boundary layer clouds on the tropical circulation (Fermepin and Bony 2014), the influence of ACRE at all atmospheric levels on both the tropical and extratropical circulation (Li et al. 2015), and the influence of ACRE on the tropospheric circulation response to climate change (Voigt and Shaw 2015, 2016; Merlis 2015).

In this contribution, we highlight the influence of ACRE on the stratospheric circulation, which to our knowledge has not been emphasized in previous work. The current study may be viewed as a companion study to Li et al. (2015). In that study, we demonstrated that ACRE have a robust influence on the simulated atmospheric circulation throughout the global troposphere. Here we demonstrate that ACRE also have a robust influence on the global stratospheric circulation.

2. Numerical experiments

There are two commonly applied methodologies for assessing the influence of cloud radiative effects on the atmospheric circulation in numerical simulations. One is to fix cloud radiative properties to their control values at every call in the radiation code (the "cloud-locking" method). The locking method has been used to quantify various radiative feedbacks (e.g., Wetherald and Manabe 1980, 1988; Hall and Manabe 1999; Schneider et al. 1999; Mauritsen 2013), to isolate the atmospheric circulation response to cloud radiative effects from the direct radiative forcing of $4\times CO2$ (Ceppi and Hartmann 2016; Voigt and Shaw 2016), and to explore the climate response to the suppression of cloud/circulation interactions (Rädel et al. 2016). A second method is to turn off cloud radiative effects at every call in the radiation code (e.g., Slingo and Slingo 1988; Randall et al. 1989; Slingo and Slingo 1991; Stevens et al. 2012; Fermepin and Bony 2014; Crueger and Stevens 2015; Li et al. 2015; Merlis 2015; Harrop and Hartmann 2016). The second approach induces large changes in the top of the atmosphere radiative fluxes, hence it is typically applied in simulations runs with prescribed sea-surface temperatures (SSTs) to avoid climate drift. Fixing SSTs minimizes the effects of changes in surface cloud radiative effects, and thus the second approach emphasizes the role of longwave atmospheric cloud radiative effects on the circulation.

Here we exploit the second approach to explore the influence of ACRE on the long-term mean stratospheric flow. To do so, we exploit output of AMIP-type numerical experiments conducted under the auspices of the COOKIE experiments. Details of the experiments are provided in Appendix A and Stevens et al. (2012). In brief, the COOKIE project provides a framework for exploring the circulation response to ACRE in a variety of numerical models and experiment set-ups (Stevens et al. 2012). We focus on two AMIP-type experiments from the atmospheric component of the Institut Pierre Simon Laplace (IPSL) coupled climate model (version IPSL-CM5A-LR;

Dufresne et al. 2013): 1) a 30-yr control "clouds-on" experiment in which the full suite of ACRE are included in the simulations and 2) a 30-yr "clouds-off" experiment in which model ACRE are turned off in the radiative code. The two experiments are forced by the same observed monthly-mean SSTs and sea-ice concentrations over the period 1979–2008. Thus, the differences between clouds-on and clouds-off experiments uniquely reveal the impact of ACRE on the model climate given identical surface boundary conditions. The robustness of the primary results in other numerical models available through the COOKIE project is reviewed in the Discussion.

Figure 1 briefly reviews the long-term mean atmospheric circulation derived from the "clouds on" simulation (left panels) and compares it with that derived from European Centre for Medium-Range Weather Forecasts interim reanalysis (ERA-Interim; Simmons et al. 2007). Details of the calculation of the fields shown in Fig. 1 are given in Appendix B. The climatological-mean circulation of the atmospheric component of the IPSL coupled climate model was also reviewed in Li et al. (2015), but the discussion there focused on circulation features at tropospheric levels. Here we focus on the circulation at stratospheric levels.

The key point in Figure 1 is that the atmospheric component of the IPSL model closely captures key aspects of the climatological-mean stratospheric circulation. These include (e.g., Andrews et al. 1987):

- westerly jets at mid-high latitudes that extend poleward and upward from the midlatitude tropopause in both hemispheres (Figs. 1a,b). The relatively weak amplitude of the Northern Hemisphere polar vortex reflects hemispheric differences in stratospheric wave drag due to upward propagating, hemispheric-scale Rossby waves (Figs. 1e,f).

- equator-to-pole residual mass overturning cells in both hemispheres, with upwelling at the tropical tropopause and downwelling in the mid-high latitude stratosphere (Figs. 1c,d). Both

the model and observed Brewer-Dobson circulations are centered slightly north of the Equator in the annual-mean.

- vertically propagating wave activity at stratospheric levels that bends equatorward in the middle stratosphere and dissipates at both subtropical and extratropical latitudes (Figs. 1e,f). The wave dissipation is the principal forcing of the stratospheric residual circulation indicated in panels c and d (e.g., Andrews et al. 1987; Haynes et al. 1991).

3. The influence of ACRE on the stratospheric circulation

Figure 2 shows the simulated ACRE in the IPSL model. The figure is reproduced from Li et al. (2015) and shows only the longwave component of the ACRE, since it dominates the cloud radiative forcing within the atmosphere. As discussed in Li et al. (2015), the primary features in the zonal-mean ACRE include 1) radiative cooling in the upper troposphere near the tropopause level due to the emission of longwave radiation from cloud tops, and 2) radiative warming the middle troposphere due to the trapping of outgoing longwave radiation by middle- and upper-level clouds.

Figures 3-5 show the differences in various key fields when the ACRE indicated in Fig. 2 are included in the radiation code. Since all fields other than ACRE are held fixed between the two runs, the "clouds-on" − "clouds-off" results shown in Figs. 3-5 reflect the influence of ACRE on the model circulation. Figure 3 shows the differences in zonal-mean temperature, zonal-mean zonal wind, and the residual mass streamfunction; Figure 4 shows the differences in the EP flux and its divergence, the eddy fluxes of heat, and the eddy fluxes of momentum; and Figure 5 shows the differences in static stability and cloud fraction.

The tropospheric response to ACRE is discussed in Li et al. (2015) and consists primarily of 1) increases in the meridional temperature gradient and thus baroclinicity in the sub-tropical up-

per troposphere (Fig. 3a); 2) anomalous westerly flow centered $\sim$40° and easterly flow centered $\sim$65° (Fig 3b); 3) anomalously poleward eddy heat fluxes in the upper troposphere at midlatitudes (Fig. 4b); and 4) anomalously poleward eddy momentum fluxes south of $\sim$45°, and anomalously equatorward eddy momentum flux north of $\sim$45° (Fig. 4c).

The stratospheric component of the response to ACRE is clearly substantial but has not been explored in previous work. The primary differences in the stratospheric flow include:

- cooling in the lower stratosphere at tropical latitudes centered around $\sim$70 hPa, juxtaposed against relatively weak warming at high latitudes above 70 hPa (Fig. 3a).

- decreases in static stability in the upper troposphere juxtaposed against increases in static stability in the lower stratosphere (Fig. 5a). The changes in the static stability derive primarily from the cooling of the lowermost stratosphere (Fig. 3a) and reflect a strengthening and upward shift of the tropopause inversion layer (TIL; Birner et al. 2002; Birner 2006).

- widespread increases in cloud fraction near the tropopause (Fig. 5b). As noted in Li et al. (2015), the changes in cloud fraction are consistent with the local decreases in static stability (Fig. 5a) and rising of the tropopause (see Fig. 3a). As discussed later, they likely play an important role in radiative coupling between the model stratospheric and tropospheric circulations.

- westerly changes in the zonal flow centered around 30–40° juxtaposed against easterly changes around 70° (Fig. 3b). The changes in the stratospheric flow indicate a weakening and slight equatorward shift of the stratospheric polar vortices.

- increases in upwelling in the tropical stratosphere juxtaposed against enhanced downwelling at extratropical latitudes (Fig. 3c). The changes in the stratospheric mass streamfunction reflect a 20% strengthening of the model BDC.

- increases in the vertical flux of wave activity (and thus the meridional eddy heat flux) in the lower extratropical stratosphere (Figs. 4a,b).

- changes in meridional wave propagation (and thus the meridional eddy momentum flux) within the stratosphere. Waves are bent anomalously equatorward to the south of $\sim 45^{\circ}$ and anomalously poleward at high latitudes (Figs. 4a,c).

What physical processes drive the changes in the model stratospheric circulation that result from the inclusion of ACRE? The changes in the stratospheric circulation shown in Figs. 3-5 can be viewed in the context of two components: 1) a *dynamical* component that is consistent with the changes in the fluxes of wave activity both into the lower stratosphere and within the stratosphere, and 2) a *radiative* component that is consistent with the changes in the flux of longwave radiation into the lower stratosphere.

Much of the response in the stratospheric zonal flow and meridional overturning circulation to ACRE are consistent with the *dynamical* component. The amplitude of the stratospheric meridional overturning circulation is linked to the propagation of both synoptic and planetary scale waves into the extratropical stratosphere, and different wave types play different roles in driving the circulation at different levels (e.g., Yulaeva et al. 1994; Randel et al. 2008; Ueyama and Wallace 2010; Birner and Boñisch 2011; Ueyama et al. 2013; Grise and Thompson 2013). The strengthening of the model BDC, the cooling of the tropical stratosphere, the relatively weak warming of the high latitude stratosphere above 70 hPa, and the easterly changes in the high latitude flow are all consistent with the enhanced vertical flux of wave activity from the troposphere into the lower stratosphere (Figs. 4a,b). The westerly anomalies in the midlatitude stratosphere (Fig. 3b) are consistent with the anomalous poleward momentum fluxes centered near 30-40°, which arise from the anomalous equatorward refraction of stratospheric wave fluxes at low latitudes (Figs. 4a,c).

The enhanced vertical flux of wave activity from the troposphere into the lower stratosphere is consistent with the increases in baroclinicity and thus wave amplitudes in the subtropical and middle latitude upper troposphere (see also Li et al. 2015). The increases in upper tropospheric baroclinicity are, in turn, driven directly by the meridional structure of the ACRE, e.g., above 400 hPa, the ACRE heat the free troposphere at low latitudes but cool it at high latitudes (Fig. 2). Similar reasoning has been applied to the simulated response of the BDC to tropical tropospheric warming (Eichelberger and Hartmann 2005) and increases in atmospheric greenhouse gases (e.g., Wang et al. 2012). The changes in the refraction of the EP flux in the low latitude stratosphere (which are also reflected in the changes in the eddy momentum fluxes) are presumably linked to changes in the meridional and vertical gradients of the stratospheric flow (e.g., Matsuno 1970), but a detailed analysis of the index of refraction is beyond the scope of this study.

The cooling of the extratropical lower stratosphere and the associated changes in near tropopause static stability are consistent with the radiative component of the stratospheric response. (The cooling of the extratropical lowermost stratosphere is the opposite sign of that expected from the changes in the BDC, and thus can not be driven by the changes in stratospheric wave drag). That is: The pattern of ACRE includes large cooling in the extratropical upper troposphere (Fig. 2) where the upward emission of longwave radiation by cloud tops exceeds the incident radiation from above. The inclusion of ACRE in the "clouds on" simulation thus acts to decrease static stability near the extratropical tropopause which, in turn, leads to increases in cloud fraction there (Fig. 5b, see also the discussion in Li et al. 2015). The increases in cloud fraction lead to an increase in the radiative cooling of the extratropical tropopause and thus to cooling of the extratropical lower stratosphere (Fig. 4b). As discussed further in Section 4, the increases in cloud fraction near the extratropical tropopause also contribute to a shortening of the radiative timescales in the lowermost stratosphere.

The radiative and dynamical forcing of the stratospheric circulation induced by ACRE is not uniform throughout the year. Figure 6 highlights the seasonal cycle of the dynamical and radiative components of the forcing. Figure 6a shows the seasonal cycle of the differences in cloud longwave heating rate at 300 hPa; Figure 6b the differences in the vertical flux of wave activity into the lower stratosphere (i.e., the vertical component of the EP flux at 100 hPa) and Figure 6c the differences in cloud fraction at 250 hPa. At extratropical latitudes, the changes in longwave heating rates in the upper troposphere, cloud incidence in the upper troposphere (which closely correspond to the changes in longwave heating rates), and the vertical flux of wave activity in the lower stratosphere all peak during the cold season months in both hemispheres. As such, the changes in the model BDC also peak during the cold seasons (not shown). At low latitudes, the positive cloud longwave heating extends further poleward during the warm season months, but otherwise exhibits a less pronounced seasonal cycle.

4. Projection onto the timescales of stratospheric variability

In this section, we examine the changes in the timescales of stratospheric dynamic variability which, in turn, are linked to the radiative timescales in the lowermost stratosphere.

Figure 7 shows the autocorrelation function of the NH extratropical zonal-mean zonal wind and temperature anomalies as a function of latitude and height for the winter season months January–March (JFM). The details of the calculation of the *e*-folding time scale are provided in Appendix B. In the clouds-on experiment, the simulated *e*-folding time scales are greatest in the extratropical zonal wind field around 55°N and 70 hPa and in the extratropical temperature field poleward of 70°N between ∼100–200 hPa. In these regions, the memory in the flow is roughly comparable to observational estimates of the timescales of the northern annular mode, or ∼40 days (Baldwin et al. 2003; Gerber et al. 2008). Interestingly, the *e*-folding autocorrelation time scale is considerably

longer in the clouds-off experiments than it is in the clouds-on experiments ($\sim$65 vs. $\sim$40 days). The persistence of the extratropical stratospheric circulation is unrealistically long in the absence of ACRE.

Understanding the timescale of the lowermost extratropical winter stratosphere has important implication for two-way coupling between the stratosphere and troposphere (Baldwin et al. 2003). The slowly varying circulations in the wintertime lower stratosphere have been shown to propagate downward into the troposphere (e.g., Kodera et al. 1990; Baldwin and Dunkerton 1999), where they contribute to the predictability of the tropospheric flow (e.g., Baldwin and Dunkerton 2001). The unrealistically long stratospheric timescales in the absence of ACRE may project onto an unrealistically persistent tropospheric response to stratosphere-troposphere coupling.

Figure 8 illustrates the effects of the contrasting stratospheric timescales in the clouds-on and clouds-off simulations on stratosphere/troposphere coupling. The figure shows zonal-mean zonal wind anomalies averaged between 55°–75°N regressed onto standardized JFM values of zonal-mean zonal wind anomalies at 10 hPa as a function of pressure level and lag. The lag regressions are based on daily anomaly data centered about the JFM season. By construction, positive anomalies in the zonal-mean zonal wind are largest at 10 hPa, day 0, and start decaying after day 0. It is evident that zonal-mean zonal wind anomalies are more persistent in the lower stratosphere in the clouds-off experiment than they are in the clouds-on experiment, and that the increased persistence of the stratospheric flow projects onto the timescales of the circulation in the middle and lower troposphere.

There are two possible reasons for the decreased timescales of the extratropical stratospheric circulation in the clouds-on experiment: 1) The lower stratospheric circulation is less quiescent with the addition of ACRE and/or 2) The lower stratospheric radiative damping time scales are shorter with the inclusion of ACRE. The former follows from the increases in vertical fluxes of

wave activity in the clouds-on simulation. The latter follows from the inverse relationship between the radiative damping time scales and the magnitude of the radiative cooling rate (see Appendix B for the derivation). The negative ACRE imposed in the upper extratropical troposphere (Fig. 2) act to enhance the amplitude of the (already negative) cooling rates in the upper troposphere. The increased amplitude of the (negative) radiative cooling rates leads to shorter radiative damping time scales in the extratropical upper troposphere and lower stratosphere which, in turn, lead to lessened persistence of the stratospheric flow. The cooler conditions in the extratropical lower stratosphere in the clouds-on experiment (Fig. 3a) also contribute to shorter radiative damping timescales, but this effect is relatively small (Appendix B).

5. Summary and Discussion

The primary impacts of atmospheric cloud radiative effects on the stratospheric circulation are summarized in Fig. 9. We have argued that the responses can be viewed in the context of a *dynamic* component and a *radiative* component.

The *dynamic* component is consistent with the enhanced flux of wave activity into the lower stratosphere (Figs. 4a,b) and changes in the meridional propagation of wave activity within the stratosphere (Figs. 4a,c) in the clouds-on simulation. The increases in the vertical flux of wave activity is consistent with enhanced tropospheric baroclinicity and wave amplitudes in the clouds-on experiment (see Li et al. 2015). They account for the strengthening of the BDC, the cooling of the tropical stratosphere, and the relatively weak warming in the high latitude stratosphere above $\sim$70 hPa (Fig. 3a). The changes in meridional wave propagation account for the meridional dipole in the zonal wind response between subtropical and high latitudes (Fig. 3b).

The *radiative* component is consistent with enhanced cloud-top longwave cooling extending across the tropopause into the lower stratosphere due to increases in cloud fraction near the

tropopause (Fig. 5b). It accounts for the cooling of the extratropical lower stratosphere, the decreases in static stability in the upper troposphere, the increases in static stability in the lower stratosphere, and a shortening of the timescales of the stratospheric variability (Figs. 3a, 5a, 7). Previous studies have suggested that the vertical structure of static stability at the tropopause level is strongly influenced by the radiative effects of water vapor (Randel et al. 2007). The results shown here suggest that the radiative effects of clouds also contribute notably to the structure of static stability in this region.

The results shown here are based on output from one GCM (IPSL-CM5A-LR). To assess the robustness of the results, we reproduced key responses in six different GCMs also available through the COOKIE experiment (Table 1). The vertically integrated ACRE are similar across all models (Fig. 10), as are key aspects of the responses highlighted here (Table 2). For example, the strengthening of the BDC, warming in the upper polar stratosphere, cooling in the tropical lower stratosphere, weakening of the polar vortex, weakening of static stability near the tropical tropopause transition layer, cooling of the extratropical stratosphere and increases in the amplitude of the TIL are all generally robust across the range of GCMs indicated in Table 2.

Previous work has established the impact of tropospheric dynamics on the stratospheric flow (e.g., Charney and Drazin 1961; Matsuno 1970), the impact of stratospheric dynamics on the tropospheric flow (e.g., Baldwin and Dunkerton 2001; Limpasuvan et al. 2004, 2005), the influence of stratospheric radiative fluxes on tropospheric temperatures (Forster et al. 2007; Grise et al. 2009), and the influence of stratospheric dynamics on tropospheric clouds (Li and Thompson 2013; Davis et al. 2013; Kohma and Sato 2014; Kodera et al. 2015). The results shown provide a novel pathway through which stratospheric and tropospheric processes are coupled: via the influence of tropospheric cloud radiative effects on stratospheric climate.

Acknowledgment. We thank Sandrine Bony (LMD) for providing the daily output "clouds-off" simulation on original vertical resolutions (39 levels).

APPENDIX A

CFMIP COOKIE simulations

The Clouds On-Off Klimate Intercomparison Experiment (COOKIE Stevens et al. 2012) is performed under the auspices of the Cloud Feedback Model Intercomparison Project (CFMIP). In the clouds-off experiment, clouds are made transparent in the call to radiation code. The clouds-on and clouds-off simulations are both run with the same sea surface temperatures. The absence of air-sea coupling has obvious limitation in reproducing the observed climate (e.g., Bretherton and Battisti 2000). Nevertheless, the COOKIE framework provides a very clean way of isolating the influence of ACRE on the circulation while holding all other variables - including SSTs - fixed.

The primary results presented in this study are based on the COOKIE simulations generated by IPSL-CM5A-LR model. The atmospheric resolution of the IPSL-CM5A-LR is 3.75° latitude $\times$ 1.875° longitude mesh, and at 39 vertical levels on a hybrid sigma pressure coordinate system with the top level extending up to 0.04 hPa. The model output used in this study are essentially the same as those used in Li et al. (2015), but unlike in Li et al. (2015), the diagnostic terms (as described in Appendix B) are calculated based on 39 original sigma levels (as opposed to the interpolated 8 pressure levels used in Li et al. 2015) so as to better represent the fine-scale vertical structure of the stratospheric response.

We also performed selected analyses for six other different models available for the COOKIE set up. The details of the models are given in Table 1.

APPENDIX B

Diagnostic details

a. Calculations of the Eliassen-Palm Flux (EP) flux

In the quasi-geostrophic (QG) approximation, the Eliassen-Palm Flux vector, **F** (hereafter EP flux), in spherical and pressure coordinates (Edmon et al. 1980; Vallis 2006) can be written as:

$$F_\phi = -a\cos\phi[v^*u^*], \tag{B1}$$

$$F_p = fa\cos\phi\frac{[v^*\theta^*]}{[\theta]_p}, \tag{B2}$$

Here the bracket (asterisk) denotes zonal means (deviation from the zonal mean). a is the radius of Earth, ϕ is latitude, $f = 2\Omega\sin\phi$ is the Coriolis parameter, u and v are the zonal and meridional velocity components. θ denotes potential temperature, and its partial derivative with respect to p is written as θ_p. The eddy fluxes are calculated based on daily-mean output and then averaged over the time period of interest.

The EP flux divergence term related to the acceleration of the zonal-mean zonal flow in the zonal-mean momentum equation is:

$$D_F \equiv \frac{1}{a\cos\phi}\nabla\cdot\mathbf{F}, \tag{B3}$$

with the flux divergence given by:

$$\nabla\cdot\mathbf{F} = \frac{1}{a\cos\phi}\frac{\partial}{\partial\phi}\left(F_\phi\cos\phi\right) + \frac{\partial}{\partial p}\left(F_p\right). \tag{B4}$$

For a graphical display of EP flux in latitude-pressure coordinates, the EP flux vectors are scaled according to Edmon et al. (1980, see Eq. 3.12). In addition, to enhance the visibility of the small vectors in the stratosphere, the EP flux is scaled by the square root of 1000/pressure (Taguchi and Hartmann 2006), and is scaled by a magnification factor of 5 above 100 mb.

Variations in the planetary wave EP flux entering the lower stratosphere are associated with changes in residual zonal-mean circulation ($[\tilde{v}]$, $[\tilde{w}]$; e.g., Haynes et al. 1991), defined by

$$[\tilde{v}] \equiv [v] - \frac{\partial}{\partial p}\left(\frac{[v^*\theta^*]}{[\theta]_p}\right), \tag{B5}$$

$$[\tilde{\omega}] \equiv [\omega] + \frac{1}{a\cos\phi}\frac{\partial}{\partial\phi}\left(\frac{[v^*\theta^*]}{[\theta]_p}\cos\phi\right). \tag{B6}$$

The quantities $[\tilde{v}]$ and $[\tilde{w}]$ are linked by a continuity equation

$$\frac{1}{a\cos\phi}\frac{\partial}{\partial\phi}([\tilde{v}]\cos\phi) + \frac{1}{\rho_0}\frac{\partial}{\partial z}(\rho_0[\tilde{w}]) = 0. \tag{B7}$$

The associated "residual" mean streamfunction $\widetilde{\Psi}_M$ is derived from the $[\tilde{v}]$ and $[\tilde{w}]$, given by

$$\widetilde{\Psi}_M = \frac{2\pi a\cos\phi}{g}\int_0^p [\tilde{v}]dp. \tag{B8}$$

In this study, the strength of the BDC is estimated from the residual mass stream function.

b. Calculation of the e-folding time scale

The *e*-folding time scale is computed following Baldwin et al. (2003) and Gerber et al. (2008). The daily time series are first applied with 10-day low-pass Lanczos filter (Duchon 1979) with 61 weights so as to remove the high frequency variability. The *e*-folding time scale (τ) is estimated by finding the best least square fit of $exp(-t/\tau)$ to the autocorrelation function of the filtered daily time series between lag zero and the point at which the autocorrelation drops to the value $\sim 1/e$ ($\sim$ 40 day lag).

c. Calculation of cooling rates and relaxation time scale

The time evolution of the atmospheric temperature can be decomposed into contributions from radiative terms and dynamic terms:

$$\left(\frac{dT}{dt}\right)_{tot} = \left(\frac{dT}{dt}\right)_{rad} + \left(\frac{dT}{dt}\right)_{dyn} \tag{B9}$$

Consider the atmosphere initially at equilibrium, thus

$$\left(\frac{dT}{dt}\right)_{tot,old} = 0. \tag{B10}$$

Then,

$$\left(\frac{dT}{dt}\right)_{rad,old} + \left(\frac{dT}{dt}\right)_{dyn} = 0 \tag{B11}$$

Suppose a small external perturbation (ΔT) on the equilibrium temperature, radiative cooling rates is changed accordingly. So the new temperature (T) relaxes at a new rate:

$$\begin{aligned}\left(\frac{dT}{dt}\right)_{tot,new} = \frac{d\Delta T}{dt} &= \left(\frac{dT}{dt}\right)_{rad,new} + \left(\frac{dT}{dt}\right)_{dyn} \\ &= \left(\frac{dT}{dt}\right)_{rad,new} - \left(\frac{dT}{dt}\right)_{rad,old} \qquad \text{(B12)} \\ &= \frac{\partial}{\partial T}\left(\frac{dT}{dt}\right)_{rad} \Delta T \qquad \text{(B13)}\end{aligned}$$

The radiatively induced time rate of change of temperature due to absorption or emission of radiation within an atmosphere layer is given by:

$$\left(\frac{dT}{dt}\right)_{rad} = \frac{g}{C_p}\frac{dF_{net}}{dp}, \tag{B14}$$

Considering an atmospheric layer, whose radiative cooling rate is dominated by the cooling-to-space mechanism (e.g., Goody and Yung 1989),

$$\begin{aligned}\left(\frac{dT}{dt}\right)_{rad} &= \frac{g}{C_p P_a}(-F^{\uparrow}) \\ &= -\frac{\varepsilon\sigma T^4}{g^{-1}C_p P_a}\end{aligned} \tag{B15}$$

where C_p is the specific heat of air, P_a is the pressure difference between the upper and lower boundaries of the layer, and g is the gravitational acceleration, $F^{\uparrow}$ is the outgoing radiation radiated by this layer, σ is the Stefan- Boltzmann constant, and ε is the effective emissivity of the layer.

Taking the temperature derivative of Eq. (B15)

$$\frac{\partial}{\partial T}\left(\frac{dT}{dt}\right)_{rad} = \frac{4\varepsilon\sigma T^3}{g^{-1}C_p P_a} \tag{B16}$$

Plug Eq. (B16) into Eq. (B13)

$$\frac{d\Delta T}{dt} = -\frac{4\varepsilon\sigma T^3 \Delta T}{g^{-1} C_p P_a} \tag{B17}$$

So the damping time scale of the temperature anomaly inferred from Eq. (B17) is:

$$\tau = (\frac{4\varepsilon\sigma T^3}{g^{-1} C_p P_a})^{-1} \tag{B18}$$

Plug Eq. (B15) into Eq. (B18):

$$\tau = \frac{T}{4}\left(\frac{dT}{dt}\right)^{-1}_{rad} \tag{B19}$$

The above estimation of the radiative relaxation time scale is accurate to the extent that the total radiative cooling can be approximated by the cooling-to-space term. While this is a generally good approximation (Goody and Yung, 1989), it neglects the additional radiative cooling (relaxation) due to radiative flux exchange between layers, and radiative flux exchange with Earth surface. Thus, this estimation offers a upper-bound estimate of the actual relaxation time.

References

Andrews, D. G., J. R. Holton, and C. B. Leovy, 1987: *Middle Atmosphere Dynamics*. Academic Press, 489 pp.

Baldwin, M. P., and T. J. Dunkerton, 1999: Propagation of the Arctic Oscillation from the stratosphere to the troposphere. *J. Geophys. Res.*, **104**, 30 937–30 946.

Baldwin, M. P., and T. J. Dunkerton, 2001: Stratospheric harbingers of anomalous weather regimes. *Science*, **294**, 581–584.

370 Baldwin, M. P., D. B. Stephenson, D. W. J. Thompson, T. J. Dunkerton, A. J. Charlton, and
371 A. O'Neill, 2003: Stratospheric memory and skill of extended range weather forecasts. *Science*,
372 **301**, 636–640.

373 Birner, T., 2006: Fine-scale structure of the extratropical tropopause region. *J. Geophys. Res.*, **111**,
374 D04 104, doi:10.1029/2005JD006301.

375 Birner, T., and H. Boñisch, 2011: Residual circulation trajectories and transit times into the extra-
376 tropical lowermost stratosphere. *Atmos. Chem. Phys.*, **11**, 817–827.

377 Birner, T., A. Dörnbrack, and U. Schumann, 2002: How sharp is the tropopause at midlatitudes?
378 *Geophys. Res. Lett.*, **29**, 1700, doi:10.1029/2002GL015142.

379 Bretherton, C. S., and D. S. Battisti, 2000: An interpretation of the results from atmospheric
380 general circulation models forced by the time history of the observed sea surface temperature
381 distribution. *Geophys. Res. Lett.*, **27**, 757–770.

382 Ceppi, P., and D. L. Hartmann, 2016: Clouds and the atmospheric circulation Response to warm-
383 ing. *J. Climate*, **29**, 783–799, doi:10.1002/2014GL060043.

384 Charney, J. G., and P. G. Drazin, 1961: Propagation of planetary-scale disturbances from the lower
385 into the upper atmosphere. *J. Geophys. Res.*, **66**, 83–109.

386 Collins, W., and Coauthors, 2008: Evaluation of HadGEM2 model. Technical Note 74, Meteoro-
387 logical Office Hadley Centrr.

388 Crueger, T., and B. Stevens, 2015: The effect of atmospheric radiative heating by clouds on the
389 Madden-Julian Oscillation. *J. Adv. Model. Earth Syst*, doi:10.1002/2015MS000434.

390 Davis, S. M., C. K. Liang, and K. H. Rosenlof, 2013: Interannual variability of tropical tropopause
391 layer clouds. *Geophys. Res. Lett.*, **40**, 2862–2866, doi:10.1002/grl.50512.

Duchon, C., 1979: Lanczos filtering in one and two dimensions. *J. Appl. Meteor.*, **18**, 1016–1022.

Dufresne, J.-L., and Coauthors, 2013: Climate change projections using the IPSL-CM5 earth system model: From CMIP3 to CMIP5. *Climate Dyn.*, **40**, 2123–2165, doi:10.1007/s00382-012-1636-1.

Edmon, H. J., B. J. Hoskins, and M. E. McIntyre, 1980: Eliassen-Palm cross sections for the troposphere. *J. Atmos. Sci.*, **37**, 2600–2616.

Fermepin, S., and S. Bony, 2014: Influence of low-cloud radiative effects on tropical circulation and precipitation. *J. Adv. Model. Earth Syst*, **06**, doi:10.1002/2013MS000288.

Forster, P. M., G. Bodeker, R. Schofield, S. Solomon, and D. W. J. Thompson, 2007: Effects of ozone cooling in the tropical lower stratosphere and upper troposphere. *Geophys. Res. Lett.*, **34**, L23 813, doi:10.1029/2007GL031994.

Gerber, E. P., S. Voronin, and L. M. Polvani, 2008: Testing the annular mode autocorrelation time scale in simple atmospheric General Circulation Models. *Mon. Wea. Rev.*, **136**, 1523–1536.

Goody, R. M., and Y. L. Yung, 1989: *Atmospheric Radiation: Theoretical Basis*. Oxford University Press, New York, NY, 544 pp.

Gordon, C., 1992: Comparison of 30-day integrations with and without cloud-radiation interaction. *Mon. Wea. Rev.*, **120**, 1244–1277.

Grise, K. M., and D. W. J. Thompson, 2013: On the signatures of equatorial and extratropical wave forcing in tropical tropopause layer temperatures. *J. Atmos. Sci.*, **69**, 857–874.

Grise, K. M., D. W. J. Thompson, and T. Birner, 2009: On the role of radiative processes in stratosphere-troposphere coupling. *J. Climate*, **22**, 4154–4161, doi:10.1175/2009JCLI2756.1.

Hall, A., and S. Manabe, 1999: The role of water vapor feedback unperturbed climate variability and global warming. *J. Climate*, **45**, 2327–2346, doi:10.1175/1520-0442(1999)012,2327:TROWVF.2.0.CO;2.

Harrop, B. E., and D. L. Hartmann, 2016: The role of cloud radiative heating in determining the location of the ITCZ in aquaplanet simulations. *J. Climate*, **29**, 2741–2763.

Haynes, P. H., M. E. McIntyre, T. G. Shepherd, C. J. Marks, and K. P. Shine, 1991: On the "downward control" of extratropical diabatic circulations by eddy-induced mean zonal forces. *J. Atmos. Sci.*, **48**, 651–680.

Hourdin, F., and Coauthors, 2013a: Impact of the LMDZ atmospheric grid configuration on the climate and sensitivity of the IPSL-CM5A coupled model. *Climate Dyn.*, **40**, 2167–2192.

Hourdin, F., and Coauthors, 2013b: LMDZ5B: The atmospheric component of the IPSL climate model with revisited parameterizations for clouds and convection. *Climate Dyn.*, **40**, 2193–2222.

Kodera, K., F. B. M., C. Claud, and N. Eguchi, 2015: The role of convective overshooting clouds in tropical stratospheretroposphere dynamical coupling. *Atmos. Chem. Phys.*, **15**, 6767–6774, doi:10.5194/acp-15-6767-2015.

Kodera, K., K. Yamazaki, M. Chiba, and K. Shibata, 1990: Downward propagation of the upper stratospheric mean zonal wind perturbation to the troposphere. *Geophys. Res. Lett.*, **17**, 1263–1266.

Kohma, M., and K. Sato, 2014: Variability of upper tropospheric clouds in thepolar region during stratosphericsudden warmings. *J. Geophys. Res.*, **119**, 10 100–10 113, doi:10.1002/2014JD021746.

Li, Y., and D. W. J. Thompson, 2013: The signature of the stratospheric Brewer-Dobson circulation in tropospheric clouds. *J. Geophys. Res.*, **118**, 3486–3494, doi:10.1002/jgrd.50339.

Li, Y., D. W. J. Thompson, and S. Bony, 2015: The influence of atmospheric cloud radiative effects on the large-scale atmospheric circulation. *J. Climate*, **28**, 7263–7278.

Limpasuvan, V., D. L. Hartmann, D. W. J. Thompson, K. Jeev, and Y. L. Yung, 2005: Stratosphere-troposphere evolution during polar vortex intensification. *J. Geophys. Res.*, **110**, doi:10.1029/2005JD006302.

Limpasuvan, V., D. Thompson, and D. Hartmann, 2004: On the life cycle of Northern Hemisphere stratosphere sudden warming. *J. Geophys. Res.*, **13**, 2584–2596.

Matsuno, T., 1970: Vertical propagation of stationary planetary waves in the winter Northern Hemisphere. *J. Atmos. Sci.*, **27**, 871–883.

Mauritsen, T., 2013: Climate feedback efficiency and synergy. *Climate Dyn.*, **41**, 2539–2554.

Merlis, 2015: Direct weakening of tropical circulations from masked CO2 radiative forcing. **112**, 13 167–13 171, doi:10.1073/pnas.1508268112.

Rädel, G., T. Mauritsen, B. Stevens, D. Dommenget, D. Dommenget, D. Matei, K. Bellomo, and A. Clement, 2016: Amplification of El Niño by cloud longwave coupling to atmospheric circulation. Nature Geoscience. *Nat. Geosci.*, **9**, 106–110.

Randall, D. A., Harshvardhan, D. A., Dazlich, and T. G. Corsett, 1989: Interactions among radiation, convection, and large-scale dynamics in a general circulation model. *J. Atmos. Sci.*, **46**, 1943–1970.

Randel, W. J., R. R. Garcia, and F. Wu, 2008: Dynamical balances and tropical stratospheric upwelling. *J. Atmos. Sci.*, **65**, 3584–3595.

Randel, W. J., M. Park, F. Wu, and N. Livesey, 2007: A large annual cycle in ozone above the tropical tropopause linked to the Brewer-Dobson circulation. *J. Atmos. Sci.*, **64**, 4479–4488.

Schneider, E. K., B. P. Kirtman, and R. S. Lindzen, 1999: Tropospheric water vapor and climate sensitivity. *J. Atmos. Sci.*, **56**, 1649–1658.

Sherwood, S. C., V. Ramanathan, T. P. Barnett, M. K. Tyree, and E. Roeckner, 1994: Response of an atmospheric general circulation model to radiative forcing of tropical clouds. *J. Geophys. Res.*, **99**, 20 829–20 845.

Simmons, A., S. Uppala, D. Dee, and S. Kobayashi, 2007: ERA-Interim: New ECMWF reanalysis products from 1989 onwards. *ECMWF Newsletter*, **110**, 25–35, ECMWF, Reading, United Kingdom.

Slingo, A., and J. M. Slingo, 1988: The response of a general circulation model to cloud longwave radiative forcing. I: Introduction and initial experiments. *Quart. J. Roy. Meteor. Soc.*, **114**, 1027–1062.

Slingo, J. M., and A. Slingo, 1991: The response of a general circulation model to cloud longwave radiative forcing. II: Further studies. *Quart. J. Roy. Meteor. Soc.*, **117**, 333–364.

Sterl, A., and Coauthors, 2012: A look at the ocean in the EC-Earth climate model. *Climate Dyn.*, **39**, 2631–2657.

Stevens, B., S. Bony, and M. Webb, 2012: Clouds on-off klimate intercomparison experiment (COOKIE). Tech. rep. [Available online at http://www.euclipse.eu/downloads/Cookie.pdf.].

Stevens, B., and Coauthors, 2013: Atmospheric component of the MPI-M earth system model: ECHAM6. Journal of Advances in Modeling Earth System. *J. Adv. Model. Earth Syst*, **5**, 146–172.

Taguchi, M., and D. L. Hartmann, 2006: Increased occurrence of stratospheric sudden warmings during El Niño as simulated by WACCM. *J. Climate*, **19**, 324–332.

Tian, B., and V. Ramanathan, 2002: Role of tropical clouds in surface and atmospheric energy budget. *J. Climate*, **15**, 296–304.

Tian, B., and V. Ramanathan, 2003: A simple moist tropical atmosphere model: The role of cloud radiative forcing. *J. Climate*, **16**, 2086–2092.

Ueyama, R., E. P. Gerber, J. M. Wallace, and D. M. W. Frierson, 2013: The role of high-latitude waves in the intraseasonal to seasonal variability of tropical upwelling in the Brewer-Dobson circulation. *J. Atmos. Sci.*, **70**, 1631–1648.

Ueyama, R., and J. M. Wallace, 2010: To what extent does highlatitude wave forcing drive tropical upwelling in the Brewer-Dobson circulation? *J. Atmos. Sci.*, **67**, 1232–1246.

Vallis, G. K., 2006: *Atmospheric and Oceanic Fluid Dynamics: Fundamentals and Large-Scale Circulation*. Cambridge University Press, Cambridge, U.K., 561 pp.

Voigt, A., and T. A. Shaw, 2015: Radiative changes of clouds and water vapor shape circulation response to global warming. *Nat. Geosci.*, **8**, 102106, doi:10.1038/ngeo2345.

Voigt, A., and T. A. Shaw, 2016: Impact of regional longwave cloud-radiative changes on the extratropical jet stream response to global warming. *J. Climate*, revised.

Voldoire, A., and Coauthors, 2013: The CNRM-CM5.1 global climate model: Description and basic evaluation. *Climate Dyn.*, **40**, 2091–212.

Wang, S., E. P. Gerber, and L. M. Polvani, 2012: Abrupt circulation responses to tropical upper-tropospheric warming in a relatively simple stratosphere-resolving AGCM. *J. Climate*, **25**, 4097–4115.

501 Wetherald, R. T., and S. Manabe, 1980: Cloud cover and climate sensitivity. *J. Atmos. Sci.*, **37**,
502 1485–1510, doi:10.1175/1520-0469(1980)037,1485:CCACS.2.0.CO;2.

503 Wetherald, R. T., and S. Manabe, 1988: Cloud feedback processes in a general circulation model.
504 *J. Atmos. Sci.*, **45**, 1397–1416, doi:10.1175/1520-0469(1988)045,1397:CFPIAG.2.0.CO;2.

505 Yukimoto, S., and Coauthors, 2012: A New Global Climate Model of the Meteorological Research
506 805 Institute: MRI-CGCM3: Model Description and Basic Performance. *J. Meteor. Soc. Japan*,
507 **90A**, 23–64.

508 Yulaeva, E., J. Holton, and J. M. Wallace, 1994: On the cause of the annual cycle in tropical
509 lower-stratospheric temperatures. *J. Atmos. Sci.*, **51**, 169–174.

LIST OF TABLES

TABLE 1. Model descriptions and details.

Modeling Center	Model Name	Atmospheric Resolution lon × lat, level	Citations
Instiut Pierre-Simon Laplace (IPSL; France)	IPSL-CM5A-LR (IPSL Coupled Model, version 5A, low resolution)	3.75° × 1.875°, L39	Dufresne et al. (2013) Hourdin et al. (2013a)
Instiut Pierre-Simon Laplace (IPSL; France)	IPSL-CM5B-LR (IPSL Coupled Model, version 5B, low resolution)	3.75° × 1.875°, L31	Dufresne et al. (2013) Hourdin et al. (2013b)
Centre National de Recherches Meteorologiques (CNRM; France)	CNRM-CM5 (CNRM Coupled Global Climate Model, version 5	1.41° × 1.40°, L39	Voldoire et al. (2013)
Met Office Hadley Centre (MOHC; U.K.)	HadGEM2-A (Hadley Global Environment Model 2-Atmosphere)	1.25° × 1.875°, L38	Collins et al. (2008)
Max Planck Institute for Meteorology (MPI-M; Germany)	ECHAM-6 (Atmospheric component of the MPI-M Earth System Model)	1.875° × 1.8653°, L31	Stevens et al. (2013)
Meteorological Research Institute (MRI; Japan)	MRI-CGCM3 (MRI Coupled General Circulation Model, version 3)	1.125° × 1.12°, L48	Yukimoto et al. (2012)
Jointly developed by several European institutes and ECMWF	EC-EARTH	1.125° × 1.12°, L62	Sterl et al. (2012)

TABLE 2. Summary statistics for the fields indicated based on seven available COOKIE models. The results are not sensitive to details of the analysis: similar results were found for averages over slightly different latitude band and vertical level. The statistical significance of the results is estimated using the Student's t statistic for the difference in means between clouds-on and clouds-off experiments. Since the results for the IPSL-CM5A-LR provide an a priori expectation of the sign of the results, confidence levels are based on a one-tailed test of the difference in sample means. Bolded values indicate where differences are significant at the 99% confidence level based on a one-tailed test of the t statistic.

	warming in the upper polar stratosphere and cooling in the lower tropical stratosphere (implying the strengthening of the BDC)		weakening of the polar vortex (implying increased wave fluxes in extratropical stratosphere)	weakening of SS near the tropical tropopause transition layer (TTL)	cooling in the extratropical lower stratosphere	strengthening of SS near the extratropical tropopause inversion layer (TIL)
Model	$[\mathrm{T}]_{10mb}^{50^\circ-70^\circ S/N}$	$[\mathrm{T}]_{70mb}^{30^\circ S-30^\circ N}$	$[\mathrm{U}]_{50mb}^{50^\circ-70^\circ S/N}$	$[N^2]_{100mb}^{30^\circ S-30^\circ N}$	$[\mathrm{T}]_{200mb}^{40^\circ-70^\circ S/N}$	$[N^2]_{150mb}^{50^\circ-70^\circ S/N}$
IPSL-CM5A-LR	**4.28** / **2.39**	**−4.84**	**−3.71** / **−3.16**	**−0.51**	**−6.03** / **−6.00**	**0.39** / **0.53**
IPSL-CM5B-LR	**4.40** / **1.19**	**−5.95**	**−8.50** / **−4.51**	**−0.39**	**−3.74** / **−5.00**	**0.29** / **0.49**
CNRM-CM5	**0.96** / 0.08	**−4.75**	**−3.90** / −0.10	**−0.42**	−0.16 / **−1.30**	**0.02** / **0.05**
HadGEM2-A	**0.99** / **0.92**	**−1.47**	**−1.31** / **−1.59**	**−0.18**	**−1.07** / **−1.38**	**0.13** / **0.21**
MPI-ECHAM6	**2.68** / **1.45**	**−3.52**	**−2.75**/**−1.48**	**−0.39**	**−0.30**/**−1.23**	**0.14** / **0.25**
MRI-CGCM3	**1.35** / **1.19**	**−2.47**	0.33 / −0.80	**−0.51**	**−0.21** / 0.31	**0.03** / **0.07**
EC-Earth	**1.15** / **1.05**	1.12	**−1.07** / 0.64	**−0.18**	**−1.09** / 0.21	0.01 / 0.00

LIST OF FIGURES

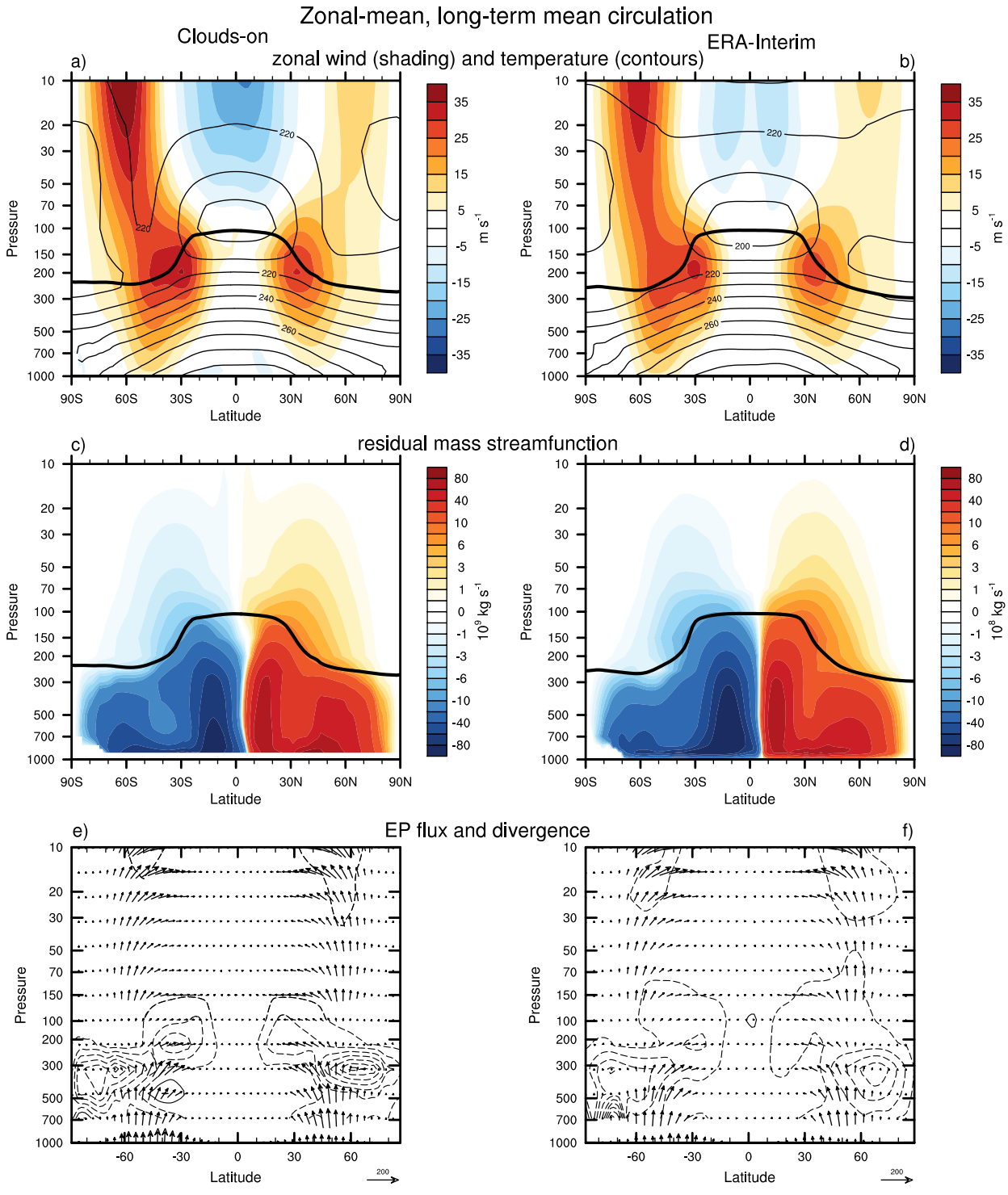

FIG. 1. Comparing the long-term mean, zonal-mean circulation of the (left) clouds-on experiment and (right) ERA-interim reanalysis for the fields indicated. The EP flux divergence is contoured at -1, 1, 3 m s^{-1} day^{-1} etc. The thick black line indicates the long-term mean tropopause height. Tropopause height is identified using the World Meteorological Organization lapse rate definition. The long-term mean denotes the mean over all 30 years (1979–2008) of the integration in the clouds-on experiment, and over the period 1979–2008 for ERA-Interim.

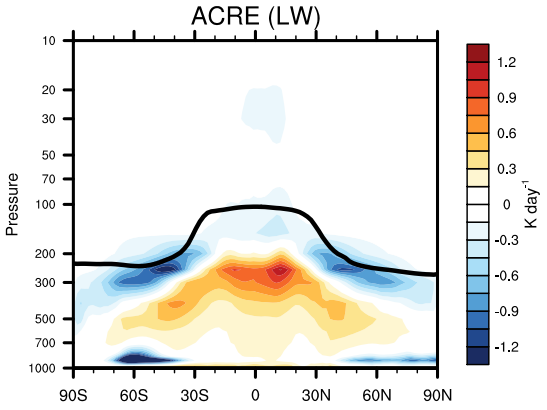

FIG. 2. The long-term-mean, zonal-mean longwave component of the atmospheric cloud radiative effects in the clouds-on experiment. The thick solid line superimposed on each panel indicates the long-term mean tropopause height in the clouds-on experiment. The results are reproduced from Li et al. (2015), but plotted in the log-pressure coordinate consistent with the following figures.

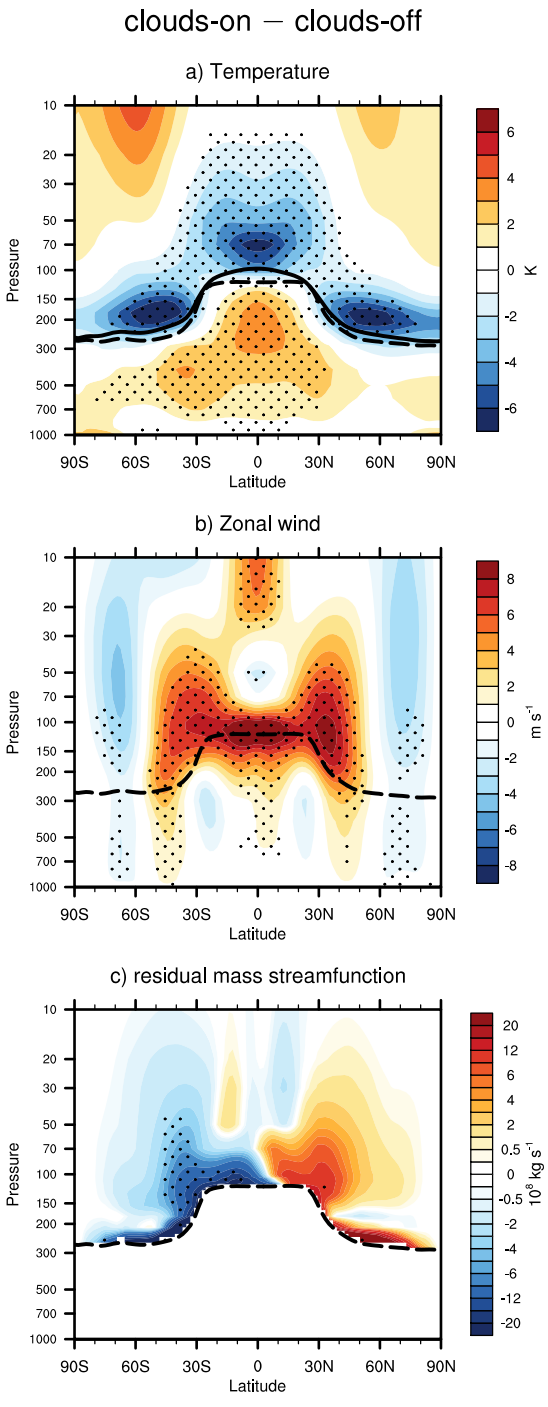

582 FIG. 3. Differences in the long-term mean, zonal-mean atmospheric circulation between the clouds-on and
583 clouds-off experiments for a) zonal-mean temperature, b) zonal-mean zonal wind, c) residual mass streamfunc-
584 tion. The dashed lines in all panels indicate the long-term mean tropopause height in the clouds-off experiment.
585 The solid line in (a) indicates the long-term mean tropopause height in the clouds-on experiment. The responses
586 in residual mass streamfunction below the tropopause are noisy and difficult to interpret, and are masked out.

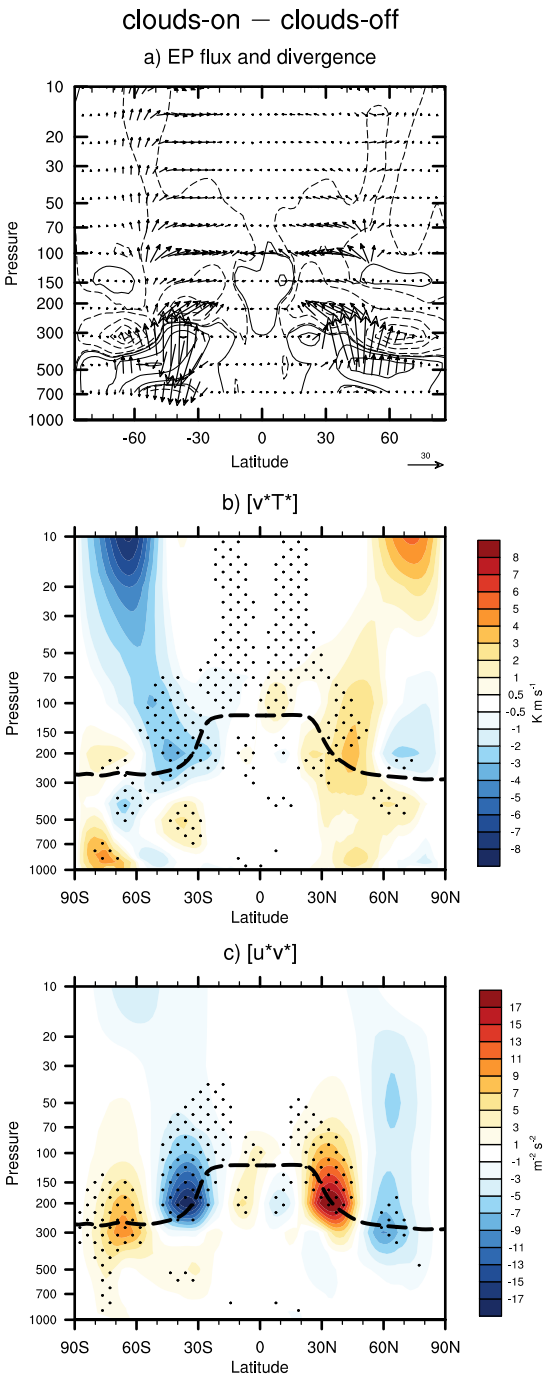

587 FIG. 4. Differences in the long-term mean, zonal-mean atmospheric circulation between the clouds-on and
588 clouds-off experiments for a) EP flux and its divergence, b) eddy flux of heat, and c) eddy flux of momentum. The
589 dashed lines in panels (b) and (c) indicate the long-term mean tropopause height in the clouds-off experiment.
590 The EP flux divergence is contoured at -5, -3, -1, -0.1, 0.1, 1, 3, 5 m s^{-1} day^{-1} etc.

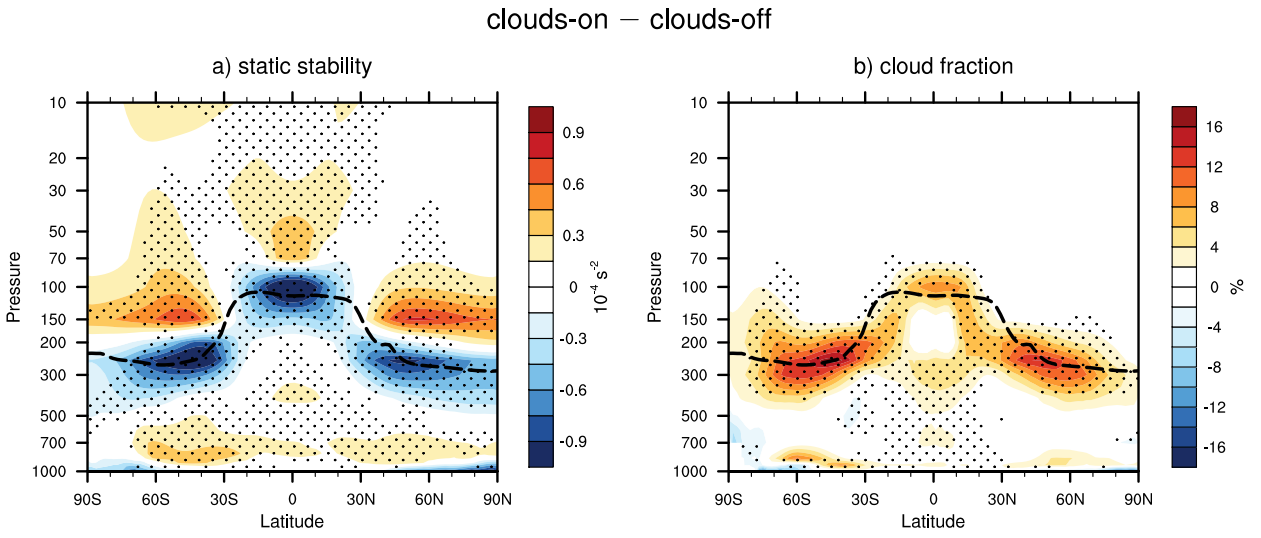

591 FIG. 5. Differences in the long-term mean, zonal-mean circulation between the clouds-on and clouds-off
592 experiments for a) static stability and b) cloud fraction. The static stability (N^2) is defined as $\frac{g}{\theta}\frac{\partial\theta}{\partial z}$, where g is
593 9.81 m s^{-2} and θ is potential temperature.

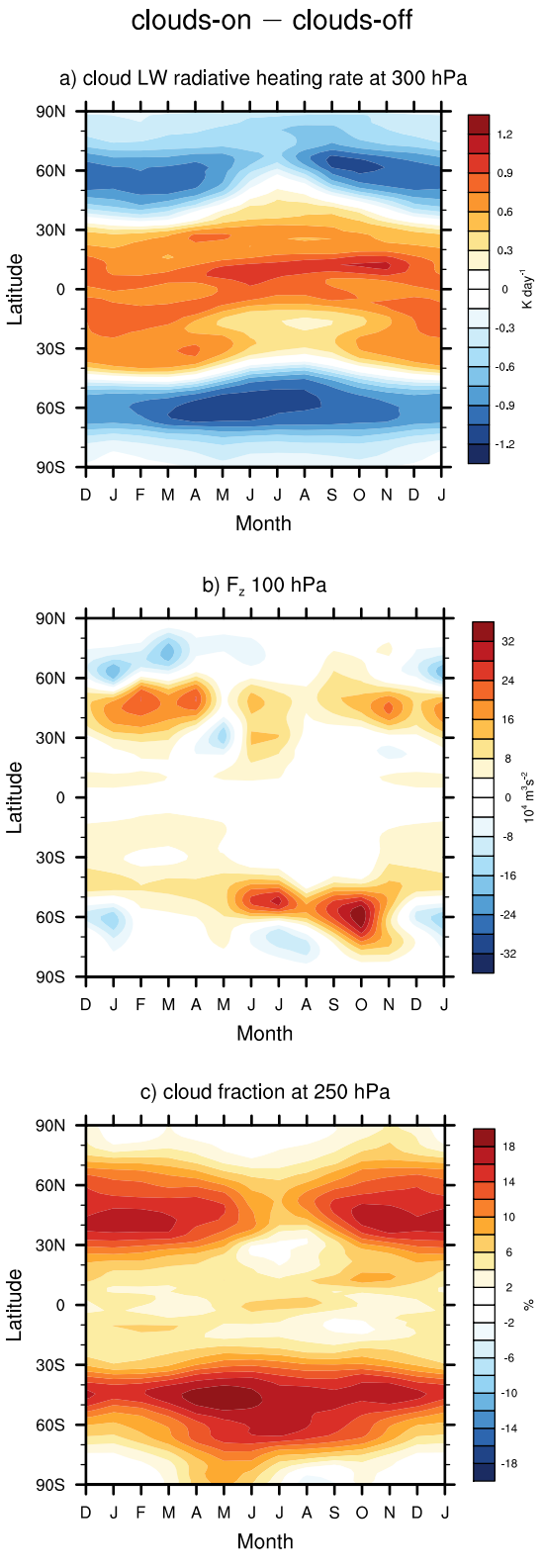

FIG. 6. Seasonal cycle of differences in the long-term mean, zonal-mean fields between the clouds-on and clouds-off experiments for a) cloud longwave radiative heating rate at 300 hPa, b) vertical component of EP fluxes at 100 hPa, and c) cloud fraction at 250 hPa.

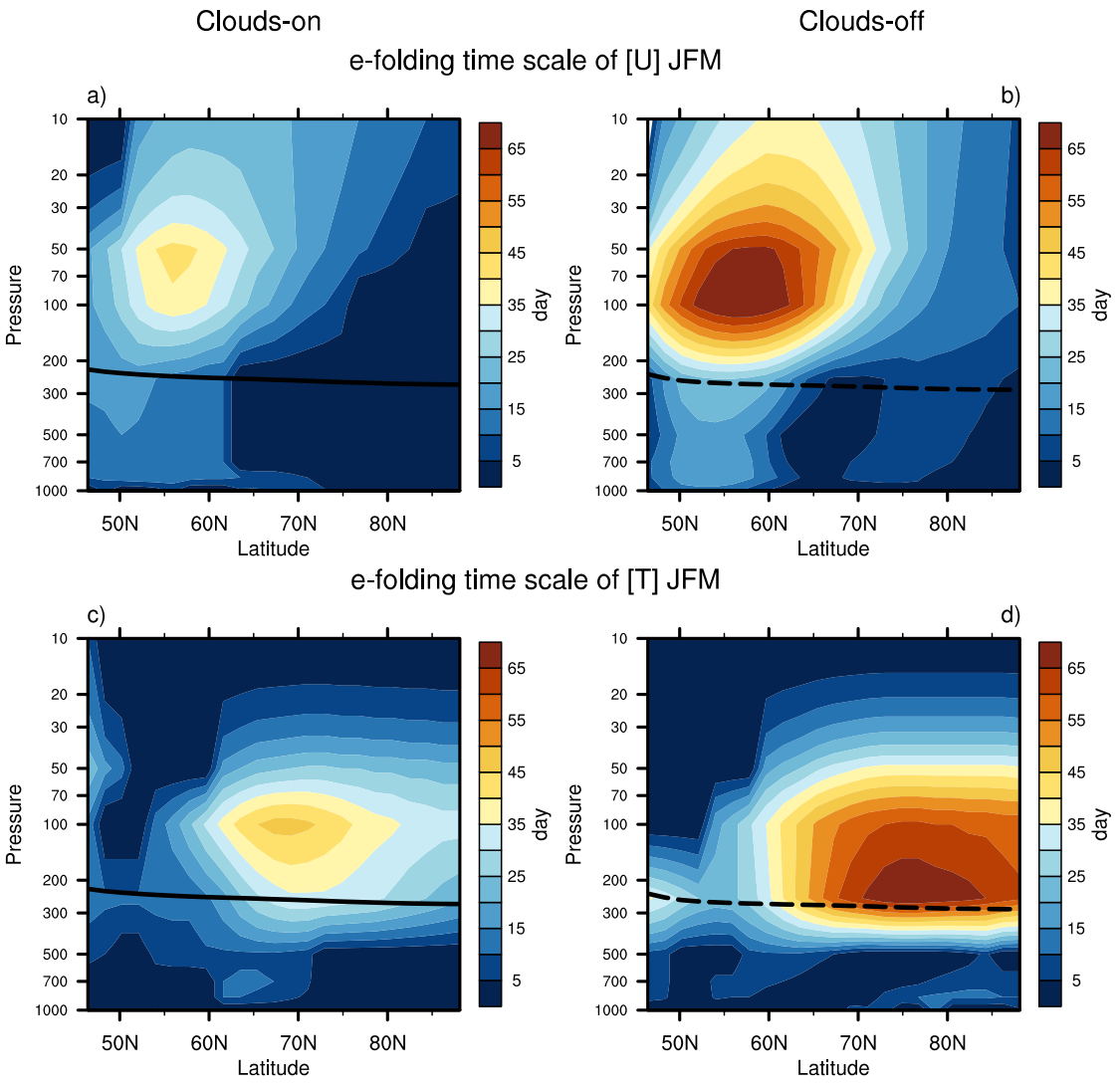

597 FIG. 7. Latitude-height cross section of the *e*-folding time scale of zonal-mean (top) zonal wind and (bottom)
598 temperatures for the winter season months January–March (JFM). Results based on the clouds-on experiments
599 are shown on the left panel, and clouds-off experiments on the right panel.

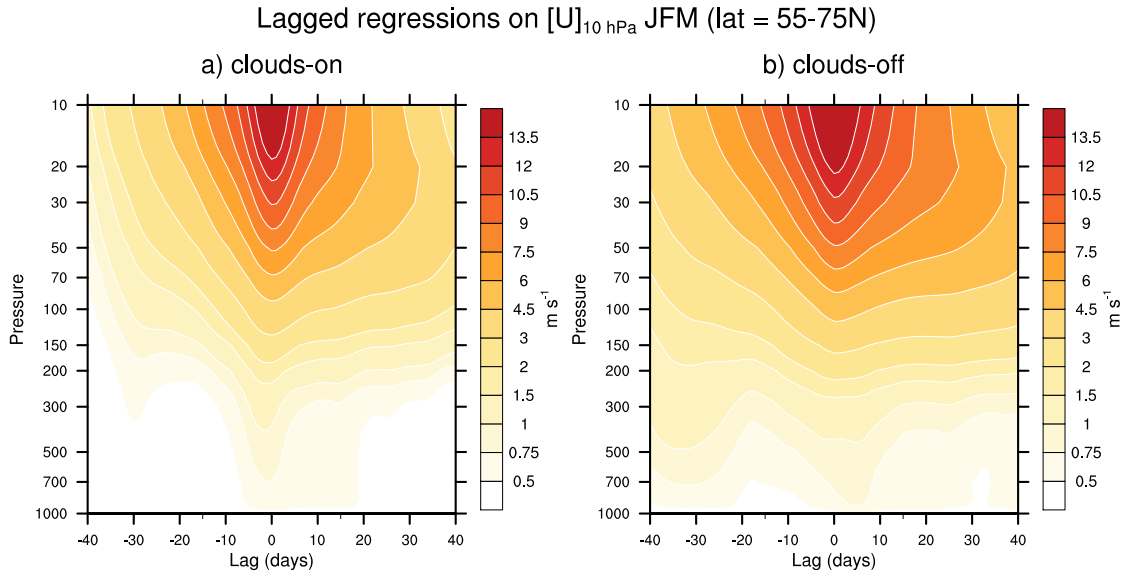

FIG. 8. Regressions of zonal-mean zonal wind anomalies averaged between 55°–75°N onto standardized values of the zonal-mean zonal wind anomalies at 10 hPa during JFM season as a function of pressure level and lag. Results based on the clouds-on experiments are shown on the left panel, and clouds-off experiments on the right panel.

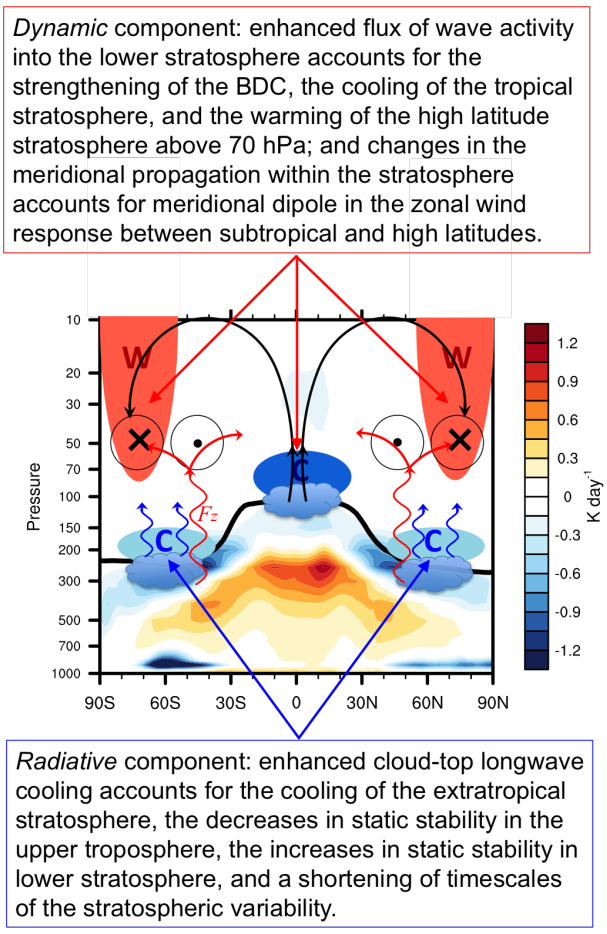

FIG. 9. Schematic diagram summarizing the basic impacts of cloud radiative effects on the zonal-mean stratospheric circulation, as revealed in this study. The background shading is reproduced from Fig. 2 and indicates the longwave component of the atmospheric cloud radiative effects in the clouds-on experiment; the solid line indicates the long-term mean tropopause height from the clouds-on experiment.

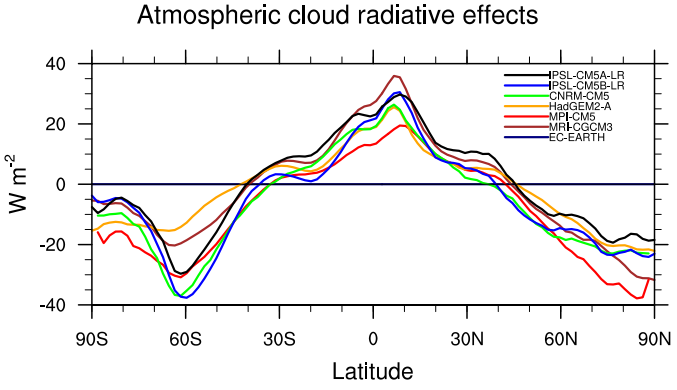

608 FIG. 10. The long-term-mean, zonal-mean, vertically integrated atmospheric cloud radiative effects in the
609 clouds-on experiment for seven models listed in Table 1.